AIAA JOURNAL
Vol. 35, No. 12, December 1997

Probability Density Functions of Acoustically Induced Strains in Experiments with Composite Plates

Alexander Steinwolf* and Robert G. White†
University of Southampton, Highfield, Southampton SO17 1BJ, England, United Kingdom

Composite structures, which are widely used in the design of flight vehicles, exhibit nonlinear behavior under in-service acoustic excitations typical of jet engine effluxes. Therefore, the responses of such structures can be non-Gaussian random processes. The dynamic strains in carbon fiber-reinforced plastic plates with clamped boundaries have been investigated experimentally in a progressive wave tube. Computer analysis concentrated on evaluation of the probability density function and its skewness and kurtosis parameters, which describe deviations from the Gaussian (normal) law model. The results show that a great lack of symmetry exists in the distribution plots of strain instantaneous values, and this influences peak probability density functions. The latter characteristic is the focus of attention for flight vehicles because it is associated directly with fatigue damage accumulation, which may be the cause of failure. The analytical description of these phenomena is also discussed. Approximation of instantaneous value distributions is made in the piecewise-Gaussain form and yields peak distribution formulas that are similarly constructed from Rayleigh law sections. The main advantage of both these solutions for experimental data fitting is that the probability density expressions obtained are convenient for use in subsequent theoretical modeling. Accuracy of the proposed method is demonstrated via a number of examples.

Nomenclature

B_j	= borders between the sections of the tetranormal probability density function
$f(s)$	= probability density of peaks in a strain response signal
M_L	= probability distribution central moment of Lth order
m	= mean value of probability distribution
n	= number of points in experimental time history records
$P(u)$	= probability density function
$P_{x\dot{x}}(u, v)$	= two-dimensional joint probability density of a strain process $x(t)$ and its derivative $\dot{x}(t)$
$R(s)$	= averaged number of positive crossings of the level s by a strain response process
V_j	= variances of sections of tetranormal probability density
$x(t)$	= time history of the strain process measured
α	= non-Gaussian parameter of tetranormal and binormal probability density functions
β	= non-Gaussian parameter of tetranormal probability density function
γ	= kurtosis of probability distribution
λ	= skewness of probability distribution
μ	= argument of the vertex point of probability density function
σ	= root mean square value of strain response signal

I. Introduction

THE use of composite materials, and particularly carbon fiber-reinforced plastics (CFRP), in the design of flight vehicles is increasing and is likely to continue to increase in future. The high modulus of elasticity of carbon fibers facilitates the construction of components with a very high stiffness-to-weight ratio. The merit of this property in relation to flight vehicles is obvious, and it is this application that has received considerable attention in recent times.[1–3] In service, vehicle components are subjected to various dynamic excitations. One of the main problems for panels is the high-frequency loading due to acoustic excitation in regions close to jet engine effluxes. Therefore, response prediction methods must be developed for CFRP structures under acoustic loads, and this necessitates the study of the nature of the dynamic behavior induced by random excitation. Most theoretical and experimental work on composite plates involves strain prediction and measurement rather than stress.

Previous studies[3–5] on the dynamic response and acoustic fatigue of CFRP plates showed that the strains induced are indicative of nonlinear behavior that is usually encountered in beam and plate structures at large deflections.[1,6,7] The main cause is geometrical nonlinearity. Small deflection linear bending theory neglects the contribution of the in-plane component to total strain energy. When the in-plane stretching effect was included in the bending formulation, the relationships for large displacement were found to be nonlinear in a manner similar to the single-degree-of-freedom Duffing system with a cubic term in the elastic force.[4,6] This term reflects an increase in, and the nonlinear nature of, the tensile forces in the midplane of the plate or beam. The result is not only that the deflections are smaller than those predicted by linear theory but a different kind of behavior also occurs. For sine excitation there is a jump of the amplitude during frequency sweeping. For broadbend random loading there is an influence of the excitation level on the shape of the response power spectrum: its peaks, corresponding to structure natural frequencies, become broader and tend to higher frequencies with the increase of excitation level. Both phenomena were observed experimentally for beams[6] and plates[5] of aluminium alloy and composite laminated materials. A principal conclusion from these studies is that for composites nonlinear behavior occurred to a greater extent than for the metallic structures.

The main peculiarity of a nonlinear system is to produce a response with extra properties absent in the loading. For sinusoidal excitation, this feature manifests itself as an appearance of higher harmonic components multiple to the driving frequency. In the case of random excitation, nonlinearity leads to transformation of the instantaneous-value distribution. Even if the noise excitation is close in its properties to the Gaussian random process, the probability density function of the response of a plate, in particular, is not adequately represented by the normal law. Therefore, to proceed from strain process measurements to their subsequent analytical modeling, for example, in fatigue prediction problems, it is often necessary to approximate the probability densities of a stationary random response in a way that describes deviations from the normal distribution.

Received Aug. 22, 1996; revision received Aug. 19, 1997; accepted for publication Aug. 26, 1997.

*Visiting Research Fellow, Department of Aeronautics and Astronautics.
†Professor, Head of the Department of Aeronautics and Astronautics.

The principal parameters characterizing non-Gaussian features of a probability density function $P(u)$ are its skewness and kurtosis

$$\lambda = M_3/(M_2)^{\frac{3}{2}}, \qquad \gamma = M_4/(M_2)^2 \tag{1}$$

governed by central moments of the distribution

$$M_L = \int_{-\infty}^{\infty} (u-m)^L P(u)\,\mathrm{d}u \tag{2}$$

The normal law

$$P_N(u) = \frac{1}{\sigma\sqrt{2\pi}} \exp\left\{-\frac{(u-m)^2}{2\sigma^2}\right\} \tag{3}$$

is described by two parameters: mean value m and variance σ^2. (The latter coincides with the second central moment M_2.) Skewness and kurtosis of the Gaussian probability density (3) are constant ($\lambda = 0$, $\gamma = 3$) and cannot be fitted to the corresponding values of the experimental distribution obtained from measurements, such as shown later.

For approximating abnormal probability densities, the Gram–Charlie and Edgeworth series, as well as Pearson and Johnson distribution families, are used.[8] After eliminating the mean value and passing to the nondimensional argument $\tilde{u} = (u-m)/\sigma$, each probability density function has two additional varied parameters to provide the prescribed skewness λ and kurtosis γ magnitudes, besides m and σ. However, at considerable non-Gaussian deviations, the truncated expansion into series form

$$P_{GC}(u) = (1/\sigma\sqrt{2\pi})\exp(-\tilde{u}^2/2)\{1 + (\lambda/6)\tilde{u}(\tilde{u}^2 - 3) + [(\gamma-3)/24](\tilde{u}^4 - 6\tilde{u}^2 + 3)\} \tag{4}$$

can create meaningless negative values at the tails of the distribution.[8,9] This is most probable when the kurtosis value γ is less than 3 as for the normal law and, consequently, the last term in expression (4) becomes negative. Furthermore, in contradiction to the behavior of strain processes in CFRP panels, the probability density function (4) may acquire extra maxima besides the main one near the mean value. The distributions of Pearson and Johnson (see Ref. 8) do not have these drawbacks. Two of them, Pearson's type IV

$$P_{\mathrm{IV}}(u) = C(1 + u^2/a^2)^{-\zeta} \exp[-b \arctan(u/a)] \tag{5}$$

and Johnson's S_u type

$$P_{Su}(u) = \frac{a(\tilde{u}^2+1)^{-\frac{1}{2}}\exp\left\{-0.5[b + a\log(\tilde{u} + \sqrt{\tilde{u}^2+1})]^2\right\}}{\sqrt{2\pi}} \tag{6}$$

have unlimited scope of argument u, which is necessary to be applicable to the problem under consideration in this paper.

Like the Gram–Charlie series (4), both approximating functions $P_{\mathrm{IV}}(u)$ and $P_{Su}(u)$ involve skewness and kurtosis, however, in implicit form through parameters C, a, b, and ζ. Moreover, these parameters cannot be expressed in analytical form. Some comments are presented in Ref. 8 about possible numerical solutions and tables available for this purpose. It is concluded in Ref. 8 that probability density functions (5) and (6) are very difficult to handle comfortably in practice. In this regard, there are some advantages in the piecewise-normal approximation procedure[10] developed for fitting symmetrical non-Gaussian distributions with various kurtosis values. This study,[10] together with that in Ref. 11 devoted to non-Gaussian aspects of ground vehicle suspension vibration, extends the approach to the case of asymmetrical distributions observed during the processing of data records of acoustically induced strains in flight vehicle components that have been obtained in the experiments described in the next section.

II. Experimental Facility and Results of Instantaneous-Value Distribution Processing

The apparatus[3,5] used for acoustic excitation experiments consisted of a large horn, which was exponential in shape about one axis and tapered along the other, with a rectangular cross section

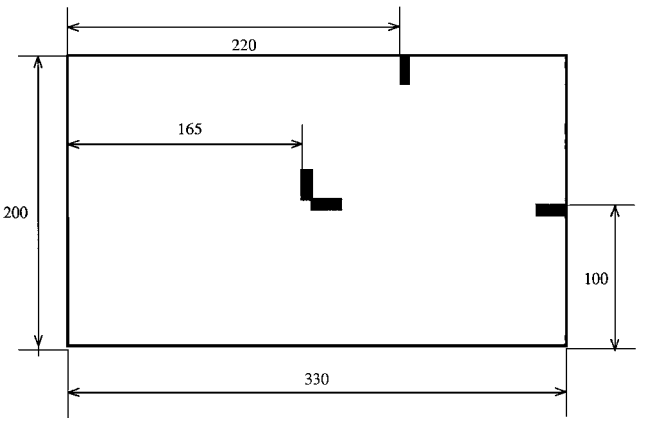

Fig. 1 Plate dimensions (in millimeters) and strain gauge locations.

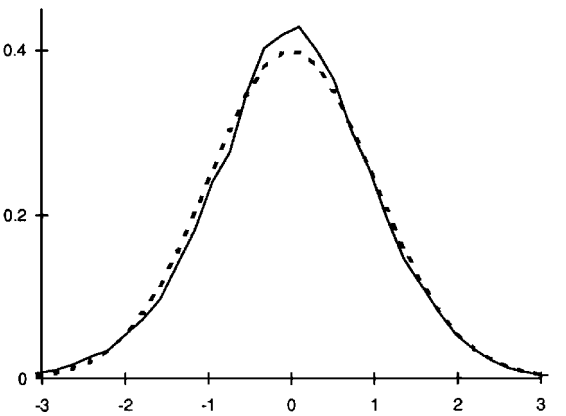

a) Sound pressure level 154 dB (kurtosis γ = 3.35)

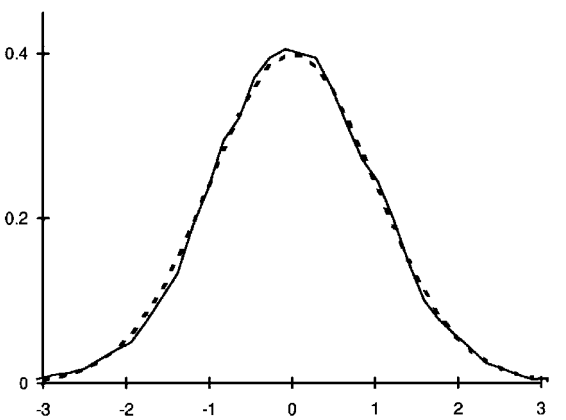

b) Sound pressure level 160 dB (kurtosis γ = 3.25)

Fig. 2 Probability density functions of the acoustic excitations generated by progressive wave tube (——) and the Gaussian law (– – –).

coupled to a tunnel. The 7.0 × 0.3 × 0.6 m tunnel was driven by an electropneumatic exciter (WAS 3000 siren) via the horn and had a sound absorbing termination at the other end. The test section had the facility for mounting test panels, clamped in steel frames, in the wall of the horn. The flat plate tested was clamped on all boundaries in the frame to give an exposed area of 330 × 200 mm (Fig. 1). The plate was constructed of eight layers of LaRC (NASA Langley Research Center)-RP46 composite material with unidirectional carbon fibers having +45-, −45-, 0-, 90-, 90-, 0-, −45-, and +45-deg orientations relative to the longer edge. The construction was cured in an autoclave, and the plate had a thickness of 1 mm and a 60% fiber volume fraction.

Sound pressure signals were acquired through a microphone mounted near the panel inside the tunnel. Resistive strain gauges, located at the center of the plate and near the clamps (Fig. 1), were used to measure the surface strains induced by the acoustic excitation

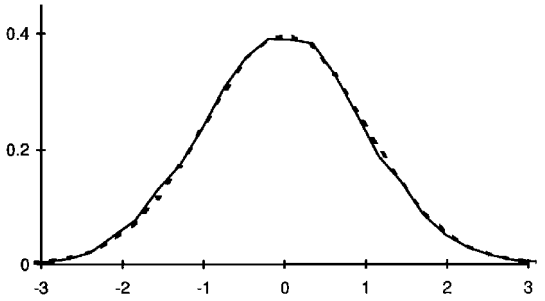

a) Sound pressure level 148 dB, horizontal gauge (skewness λ = 0.003, kurtosis γ = 3.01)

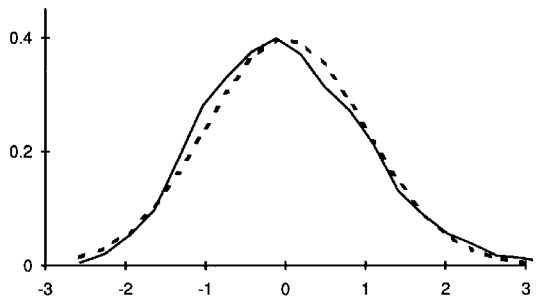

b) Sound pressure level 154 dB, vertical gauge (skewness λ = 0.30, kurtosis γ = 2.95)

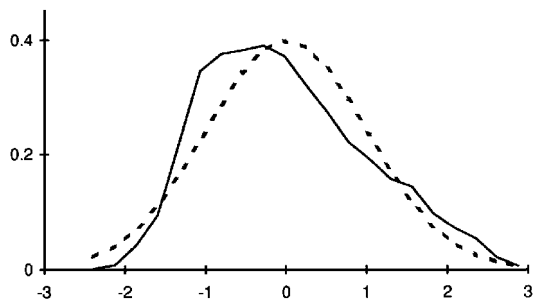

c) Sound pressure level 160 dB, vertical gauge (skewness λ = 0.45, kurtosis γ = 2.55)

Fig. 3 Strain probability distributions near the clamp (——) and the Gaussian law (– – –).

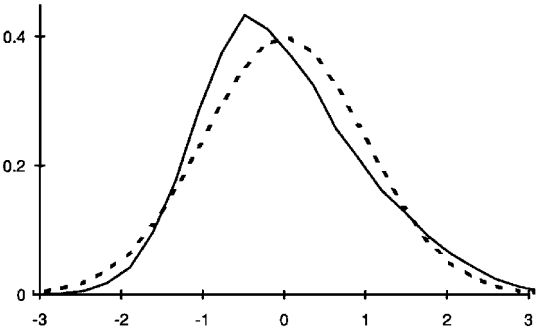

a) At the center of the plate (skewness λ = 0.5, kurtosis γ = 3.15)

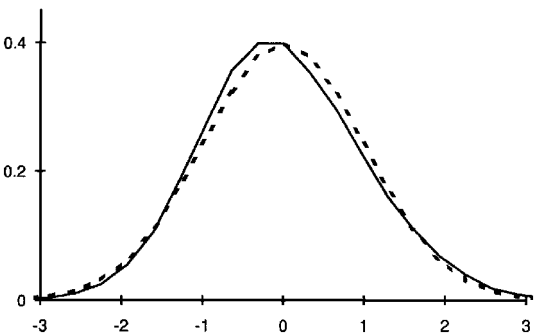

b) Near the clamp (skewness λ = 0.23, kurtosis γ = 3.05)

Fig. 4 Probability distributions of strain signals for the horizontal gauges at 150-dB sound pressure level.

with a frequency bandwidth from 80 to 800 Hz and overall sound pressure levels up to 160 dB. Excitation with such parameters is usually considered as a model of the noise produced by jet engines.[3,12] Power spectral densities of strain responses for all gauges had a peak at 200 Hz related to the first natural frequency of the plate. For vertical gauges it was the only resonance detected, and higher natural frequencies were not excited. Response signals from horizontal gauges included a noticeable contribution from the second natural frequency (about 420 Hz) in addition to the first.

The time histories of strain responses and acoustic excitation were converted from analog to digital form by the use of an HP3566A system. The data analysis algorithm concentrated on determination of the instantaneous-value probability density function as well as calculation of skewness and kurtosis values (1). The moment characteristics were found by time averaging:

$$M_L^x = \frac{1}{n}\sum_{i=1}^{n}[x(i\Delta t) - m]^L, \qquad m = \frac{1}{n}\sum_{i=1}^{n} x(i\Delta t) \qquad (7)$$

in terms of ergodic random process theory. The number of points n in time history records $x(t)$ was more than 40,000 and provided 1.3 and 2.7% accuracy of determination of skewness and kurtosis values, correspondingly. Because the step character of a histogram makes qualitative comparison with the Gaussian law curve difficult, the experimental distributions are plotted subsequently in the form of a broken line connecting the centers of vertices of the histogram rectangles. The probability density functions are presented in nondimensional form, i.e., the horizontal axis represents the ratio between instantaneous values and the rms value σ of the strain response or sound pressure.

At first, analysis of acoustic excitation data was performed to verify whether non-Gaussian behavior to be discussed was caused only by nonlinearity of the composite structure considered or, in part, also by some non-Gaussian nature of the excitation. It is evident from Fig. 2 that the probability density functions of the acoustic pressure produced by the progressive wave tube are not visibly skewed around a mean value of the distribution. Therefore, asymmetrical distortions of the distribution shape observed for all strain gauges in a greater or lesser extent were definitely caused by nonlinear behavior of the plate tested.

For low sound pressure levels, the probability density functions of strain responses were close to the Gaussian law. Figure 3a shows that such behavior still remained for some gauges at a sound pressure level of 148 dB. However, as the excitation level increased above 150 dB, nonlinear behavior of the test plate occurred and the probability distributions of instantaneous values of all response processes (examples are presented by solid curves in Figs. 3–5) changed in comparison with the normal law (dashed curve). The non-Gaussian deviations increased with increasing sound pressure level (Figs. 3b and 3c). They were dependent on the point of measurement. The probability density functions of strain processes at the center of the plate shown in Figs. 4a and 5a, appeared to be farther from the normal distribution than those near the clamp presented in Figs. 4b and 5b, correspondingly. (Figure 4 displays results for the 150-dB excitation level, and Fig. 5 is for 154 dB.)

The non-Gaussian divergence manifests itself mainly as lack of symmetry. All probability densities obtained in the experiments were skewed for the following reason. The axial strains in a vibrating plate involve only tension and, therefore, they are single sided with positive values. In consequence of this, positive values of the total strain time history (Fig. 6) exceed negative values, and as a result the instantaneous-value distribution is asymmetric. There were also some deviations in distribution sharpness. Probability density functions of the acoustic excitation (see Fig. 2) appeared to be close to the normal distribution, though slightly sharper than it (averaged kurtosis was 3.3). The strain responses tended to lesser kurtosis values related to a smoother distribution shape. This occurred for vertical

gauges (Fig. 5) more rapidly than for horizontal gauges (Fig. 4). The phenomenon can be explained in the following way. Because the plate resistance to bending loads increases when its deflection grows, high peaks in the response time history are more difficult to produce than for a linear system with constant stiffness under the same excitation. It means that the tails of the response probability density are shorter than those for the excitation, i.e., the response kurtosis is smaller.

The probability density abnormality of measured strain signals was in evidence to such an extent that the attempt to fit the experimental distribution by the Gram–Charlie truncated series (4) failed for reasons discussed in the preceding section. For example, when the skewness and kurtosis values of the experimental distribution from Fig. 5a were substituted into expression (4) unacceptable negative values appeared for nondimensional arguments $\tilde{u}$ less than -2.6 and greater than 4.8. This pitfall has been overcome via use of the piecewise-Gaussian approximation method.

III. Tetranormal and Binormal Distribution Laws

Let us construct a centralized probability density function by joining four sections of normal laws with different variances V_j shifted vertically by the value H_j and horizontally by the value A_j with respect to the coordinate origins:

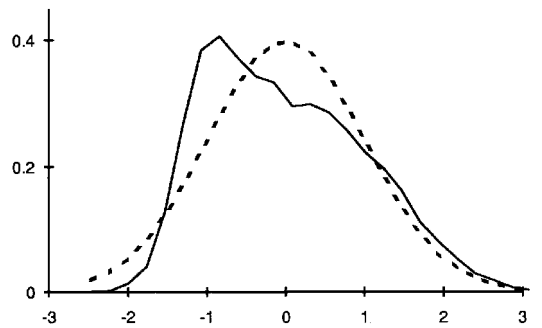

a) At the center of the plate (skewness $\lambda = 0.44$, kurtosis $\gamma = 2.5$)

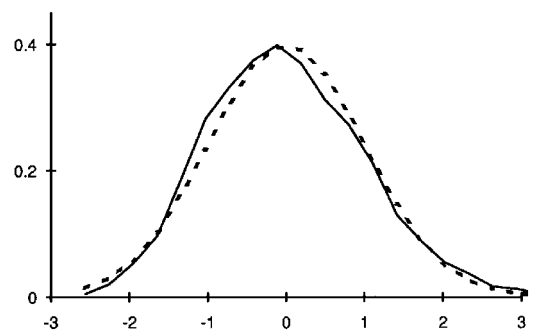

b) Near the clamp (skewness $\lambda = 0.32$, kurtosis $\gamma = 2.9$)

Fig. 5 Probability distributions of strain signals for the vertical gauges at 154-dB sound pressure level.

$$P_a(u) = \begin{cases} \dfrac{q}{\sqrt{2\pi}}\left\{\exp\left[-\dfrac{(u-A_1)^2}{2V_1}\right] + H_1\right\} & \text{at} \quad u \le B_1 \\ \dfrac{q}{\sqrt{2\pi}}\left\{\exp\left[-\dfrac{(u-A_2)^2}{2V_2}\right] + H_2\right\} & \text{at} \quad B_1 < u \le B_2 \\ \dfrac{q}{\sqrt{2\pi}}\left\{\exp\left[-\dfrac{(u-A_3)^2}{2V_3}\right] + H_3\right\} & \text{at} \quad B_2 < u \le B_3 \\ \dfrac{q}{\sqrt{2\pi}}\left\{\exp\left[-\dfrac{(u-A_4)^2}{2V_4}\right] + H_4\right\} & \text{at} \quad u > B_3 \end{cases} \tag{8}$$

The joint scale coefficient q has to be determined from the basic condition

$$\int_{-\infty}^{\infty} P_a(u)\,du = 1$$

for function (8) to be a probability density.

Suppose that the distribution under approximation is skewed and the border B_2 between the second and third sections coincides with argument μ of the distribution maximum. For the non-Gaussian case, the magnitude μ is not the same as the mean value m. To locate a vertex of the constructed probability density $P_a(u)$ at the distribution maximum point, it is necessary to set horizontal shifts A_2 and A_3 of the second and third sections equal to μ. Thereafter, the condition of continuity of the function (8) at the point $u = \mu$ also requires equating the vertical shifts $H_2 = H_3 = H$. Then, passing to other joining points B_1 and B_3 and providing continuity not only in the function $P_a(u)$ but also in its derivative, we obtain the final expression for the tetranormal probability density[11,13]

$$P_a(u, m, \sigma, \alpha, \beta) = \begin{cases} \dfrac{C}{\sigma\sqrt{2\pi}} \exp\left\{-\dfrac{[u - m - 2\sigma\alpha\rho - \sigma(Y-\beta)(Q-\alpha)]^2}{2\sigma^2 Y^2 (Q-\alpha)^2}\right\} & \text{at} \quad u - m \le \sigma D_1 \\ \dfrac{C}{\sigma\sqrt{2\pi}}\left\{\exp\left[-\dfrac{(u-m-2\sigma\alpha\rho)^2}{2\sigma^2(Q-\alpha)^2}\right] + H\right\} & \text{at} \quad \sigma D_1 < u - m \le \sigma D_2 \\ \dfrac{C}{\sigma\sqrt{2\pi}}\left\{\exp\left[-\dfrac{(u-m-2\sigma\alpha\rho)^2}{2\sigma^2(Q+\alpha)^2}\right] + H\right\} & \text{at} \quad \sigma D_2 < u - m \le \sigma D_3 \\ \dfrac{C}{\sigma\sqrt{2\pi}} \exp\left\{-\dfrac{[u - m - 2\sigma\alpha\rho + \sigma(Y_A-\beta)(Q+\alpha)]^2}{2\sigma^2 Y^2 (Q+\alpha)^2}\right\} & \text{at} \quad u - m > \sigma D_3 \end{cases} \tag{9}$$

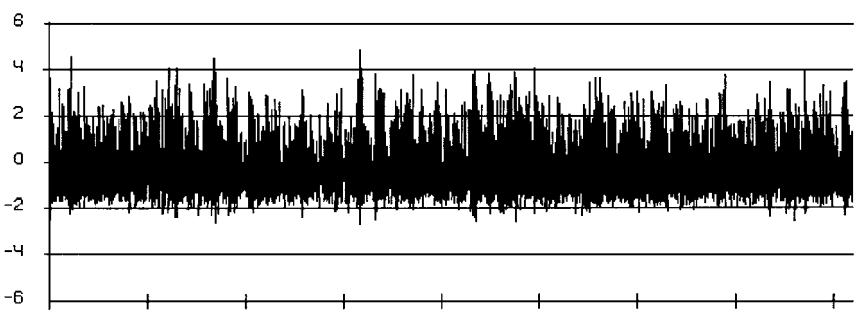

Fig. 6 Time history of a strain signal with an asymmetrical non-Gaussian probability distributions. (The data are presented on a nondimensional scale after elimination of the mean value.)

where all coefficients C, ρ, Y, Q, H, D_j presented in Ref. 11 are functions of two independent parameters α and β, which are additional in comparison with the Gaussian law (3). Therefore, it becomes possible to approximate empirical distributions not only by mean value m and variance σ^2 but also in terms of skewness and kurtosis. For this purpose formulas for skewness λ_a and kurtosis γ_a of the tetranormal law (9) in terms of its α and β parameters have been derived:

$$\lambda_a = \frac{1}{\sigma^3}\int_{-\infty}^{\infty}(u-m)^3 P_a(u)\,du = -2\alpha\frac{\{[E(\beta)]^2 b(\beta) + 4\alpha^2[z(\beta) - b(\beta)g(\beta)]\}}{G(\beta)} \tag{10}$$

$$\gamma_a = \frac{1}{\sigma^4}\int_{-\infty}^{\infty}(u-m)^4 P_a(u)\,du = \frac{C}{\sqrt{2\pi}}\left\{\left(D_3^5 - D_1^5\right)\frac{H}{5} + r_1\left(\omega_R^5 + \omega_L^5\right) + r_2\left(\omega_R^4 h_R - \omega_L^4 h_L\right) + r_3\left(\omega_R^3 h_R^2 + \omega_L^3 h_L^2\right) + r_4\left(\omega_R^2 h_R^3 - \omega_L^2 h_L^3\right) + r_5\left(\omega_R h_R^4 + \omega_L h_L^4\right) + \alpha r_6\left(\omega_R^4 - \omega_L^4\right) + \alpha^2 r_7\left(\omega_R^3 + \omega_L^3\right) + \alpha^3 r_8\left(\omega_R^2 - \omega_L^2\right) + \alpha^4 r_9(\omega_R + \omega_L)\right\} \tag{11}$$

where expressions for $E(\beta)$, $g(\beta)$, and $G(\beta)$ can be found in Ref. 11 and other coefficients are as follows:

$$z(\beta) = \rho^2\{\rho\Phi(\beta) - 3[\exp(-\beta^2/2) + 1 + Y^2 e^{-0.5}] + Y[\sqrt{\pi/2} - \Phi(1)][\rho + 3(Y-\beta)]\} + \beta\rho(\rho-\beta)(2\rho-\beta)(H/2) - y(\beta)$$

$$y(\beta) = \beta^3(2\rho-\beta)(H/4) + 3Y^2(Y\beta - \beta^2 - Y^2)e^{-0.5} + (\beta^2+2) \times \exp(-\beta^2/2) + Y[\sqrt{\pi/2} - \Phi(1)](Y-\beta)(4Y^2 - 2Y\beta + \beta^2) - 2$$

$$b(\beta) = 3\rho\{\Phi(\beta) - \beta\exp(-\beta^2/2) + Y^2(2\beta - Y)e^{-0.5} + Y[\sqrt{\pi/2} - \Phi(1)](2Y^2 - 2Y\beta + \beta^2)\} - 2y(\beta)$$

$$r_1 = 3\Phi(\beta) - \beta(\beta^2+3)\exp(-\beta^2/2) + 4Y^5 e^{-0.5} + 3Y^5[\sqrt{\pi/2} - \Phi(1)] \tag{12}$$

$$r_2 = 12Y^4 e^{-0.5}, \qquad r_3 = 6Y^3[e^{-0.5} + \sqrt{\pi/2} - \Phi(1)]$$

$$r_4 = 4Y^2 e^{-0.5}, \qquad r_5 = Y[\sqrt{\pi/2} - \Phi(1)]$$

$$r_6 = 8\rho[(\beta^2+2)\exp(-\beta^2/2) + 2]$$

$$r_7 = 24\rho^2[\Phi(\beta) - \beta\exp(-\beta^2/2)]$$

$$r_8 = 32\rho^3[\exp(-\beta^2/2) - 1]$$

$$r_9 = 16\rho^2\Phi(\beta), \qquad \omega_R = Q + \alpha, \qquad \omega_L = Q - \alpha$$

$$h_R = -\omega_R(Y-\beta) - 2\alpha\rho, \qquad h_L = \omega_L(Y-\beta) - 2\alpha\rho$$

The tetranormal asymmetric probability density $P_a(u)$ constructed is rigorously positive and has only one vertex for any permissible values of λ and γ. The distribution degenerates into the normal law when $\alpha = 0$ and $\beta = 1$.

The intermediate, partial type of piecewise-Gaussian law appears if the β parameter is fixed and only α is varied. It means that instead of there being four sections in expression (9) there are only two:

$$P_{a2}(u, m, \sigma, \alpha) = \begin{cases} \dfrac{1}{Q\sigma\sqrt{2\pi}}\exp\left[-\dfrac{(u-m-\sigma\nu)^2}{2\sigma^2(Q-\alpha)^2}\right] & \text{at} \quad u \le m + \sigma\nu \\ \dfrac{1}{Q\sigma\sqrt{2\pi}}\exp\left[-\dfrac{(u-m-\sigma\nu)^2}{2\sigma^2(Q+\alpha)^2}\right] & \text{at} \quad u > m + \sigma\nu \end{cases} \tag{13}$$

imposed on horizontal shifts without any vertical change. By this, the possibility of simultaneous kurtosis simulation is lost but simplification of skewness approximation is possible. The coefficients of the binormal law (13) depend on the one non-Gaussian parameter α according to the following expressions:

$$\nu = -\alpha\sqrt{8/\pi}, \qquad Q(\alpha) = \sqrt{1 + [(8/\pi) - 3]\alpha^2} \tag{14}$$

IV. Application of Piecewise-Gaussian Laws and Results of Fitting Instantaneous-Value Probability Distributions of Strain Responses

The formulas (10) and (11) give a possibility of determining kurtosis and skewness magnitudes for tetranormal probability densities with prescribed values of their parameters. However, for approximation of experimental distributions it is necessary to consider the contrary problem and find parameters α and β of the analytical law (9) starting from kurtosis γ_x and skewness λ_x values of the histogram. For this objective, the set of two nonlinear equations

$$\lambda_a(\alpha, \beta) = \lambda_x, \qquad \gamma_a(\alpha, \beta) = \gamma_x \tag{15}$$

has to be solved with left-hand sides governed by formulas (10–12). Then the remaining coefficients C, ρ, Y, Q, H, and D_j in formula (9) are calculated with assistance of relationships from Ref. 11.

Computer tests of the developed piecewise-Gaussian laws have shown that they provide combinations of kurtosis γ and skewness λ values (Fig. 7a) unachievable for Pearson's IV type (5) and Johnson's S_u type (6) distributions with unlimited range of change of argument (Fig. 7b). Kurtosis values less than 3 have become available with the use of tetranormal probability densities. This should be emphasized because they are inherent in most of the strain response distributions in the CFRP plates tested (see Figs. 3b, 3c, and 5).

The binormal distribution (13) does not involve a kurtosis value and provides just skewness simulation. As a consequence, the set of equations (15) transforms only to the first equation simplified with $\beta = 1$. Its solution yields the following expression for determining the single non-Gaussian parameter α in terms of the prescribed skewness value λ_x:

$$\alpha = \sqrt{\frac{\pi}{6(\pi-3)}}\cos\left\{\frac{1}{3}\arccos\left[\frac{3}{2}\lambda_x\sqrt{3(\pi-3)}\right] + \frac{4}{3}\right\} \tag{16}$$

Combination of skewness and kurtosis magnitudes created by such an approximation is shown by a line (dashed curve in Fig. 7a) and not by an area as with the more general tetranormal law.

Accuracy of the proposed method gained during approximation of the considered distributions of CFRP plate strain responses is shown in Fig. 8. An experimental probability density function from the vertical gauge at the center of the plate under 154-dB excitation is compared with a normal law (Fig. 8a) fitted in terms of variance only and with the tetranormal law (Fig. 8c) fitted in terms of variance,

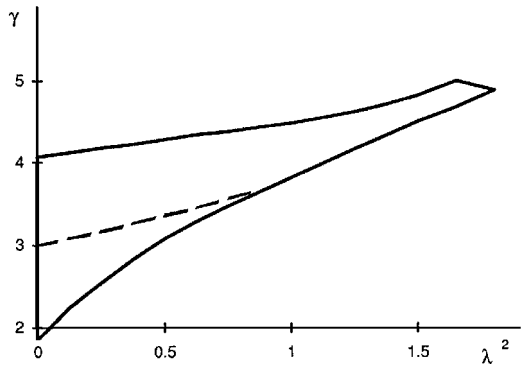

a) Tetranormal law (within the solid curve) and binormal law (along the dashed curve)

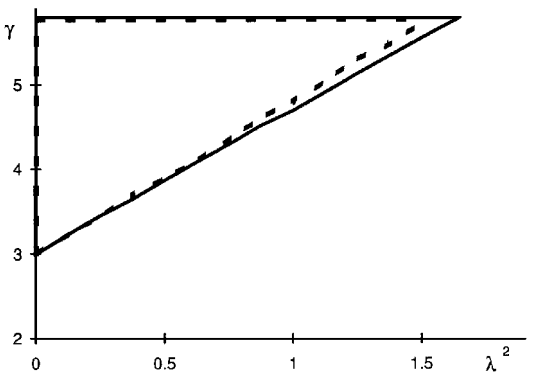

b) Pearson law (within the dashed curve) and Johnson law (within the solid curve)

Fig. 7 Ranges of kurtosis and skewness variations with different laws.

skewness λ, and kurtosis γ. In consequence of computation started from the required $\lambda_x = 0.44$ and $\gamma_x = 2.5$ values, the following expression for piecewise-Gaussian approximating distribution was obtained:

$$P_a(u) = \begin{cases} \dfrac{1.93}{\sigma\sqrt{2\pi}} \exp\left[-\dfrac{(u-m+1.2\sigma)^2}{0.08\sigma^2}\right] \\ \qquad\qquad \text{at} \quad u - m \le -1.66\sigma \\ \dfrac{1.93}{\sigma\sqrt{2\pi}} \left\{\exp\left[-\dfrac{(u-m+1.05\sigma)^2}{0.76\sigma^2}\right] - 0.52\right\} \\ \qquad\qquad \text{at} \quad -1.66\sigma < u - m \le -1.05\sigma \\ \dfrac{1.93}{\sigma\sqrt{2\pi}} \left\{\exp\left[-\dfrac{(u-m+1.05\sigma)^2}{19.2\sigma^2}\right] - 0.52\right\} \\ \qquad\qquad \text{at} \quad -1.05\sigma < u - m \le 2.05\sigma \\ \dfrac{1.93}{\sigma\sqrt{2\pi}} \exp\left[-\dfrac{(u-m+0.15\sigma)^2}{2.0\sigma^2}\right] \\ \qquad\qquad \text{at} \quad u - m > 2.05\sigma \end{cases} \tag{17}$$

Results of fitting by the simplified binormal distribution (13) are presented in Fig. 8b for the same experimental probability density as in Fig. 8a. As would be expected, the performance of this simulation of non-Gaussian strain behavior based on the skewness parameter only is impaired in comparison with simulation in Fig. 8c by the tetranormal law (9) taking into consideration both skewness and kurtosis. However, there is a certain improvement of approximation compared with the normal law in Fig. 8a. Furthermore, the binormal probability density constructed,

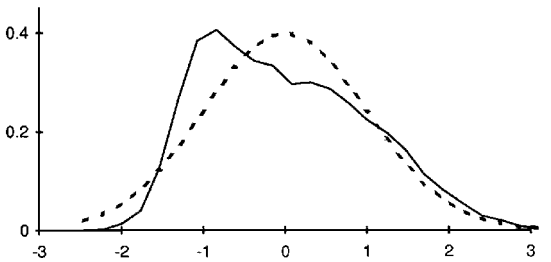

a) Experimental distribution (——) and the normal law (- - -)

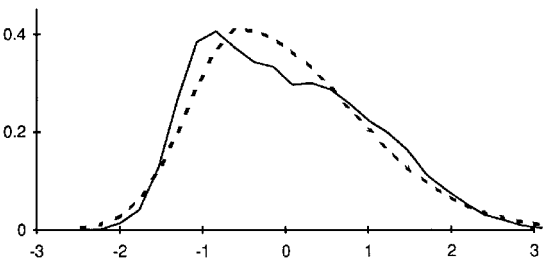

b) Experimental distribution (——) and the binormal law (- - -)

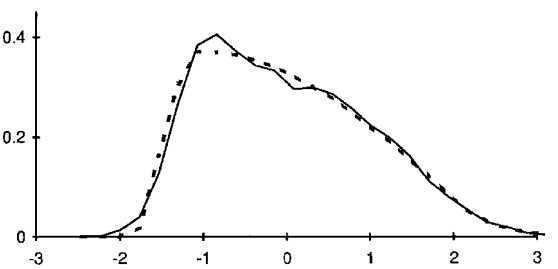

c) Experimental distribution (——) and the tetranormal law (- - -)

Fig. 8 Comparison of fitting accuracy provided by normal and piecewise-normal laws.

$$P_{a2}(u) = \begin{cases} \dfrac{1.03}{\sigma\sqrt{2\pi}} \exp\left[-\dfrac{(u-m+0.56\sigma)^2}{0.77\sigma^2}\right] & \text{at} \quad u \le m - 0.56\sigma \\ \dfrac{1.03}{\sigma\sqrt{2\pi}} \exp\left[-\dfrac{(u-m+0.56\sigma)^2}{3.5\sigma^2}\right] & \text{at} \quad u > m - 0.56\sigma \end{cases}$$

is simpler to use because it has two sections instead of four and the procedure for determining its coefficients by formulas (14) and (16) is much less difficult than by the aforementioned equations for the tetranormal distribution (9).

To quantitatively assess errors of the preceding approximation, the chi-square goodness-of-fit test was employed. According to the procedure described in Ref. 14, the discrepancy

$$X^2 = n\delta \sum_{i=1}^{K} \frac{\{p_i - P_T(u_i)\}^2}{P_T(u_i)} \tag{18}$$

was calculated between an experimental probability density given as a histogram p_i for K class intervals $[u_i - \delta/2, u_i + \delta/2]$ and the theoretical probability density function $P_T(u)$ represented by the normal (3), or tetranormal (9), or binormal (13) laws. Formula (18) gives a sample statistic, which follows the known χ^2 distribution if there is an equivalence between the analytical approximation and the measured data. The region of acceptance of this hypothesis formulated as $X^2 < \chi^2_\alpha$ is usually defined by the $\alpha = 0.05$ percentile point χ^2_α of the chi-square distribution. For the number of class intervals $K = 24$ used in our calculations, the χ^2 tables[14] give $\chi^2_{0.05} = 32.7$. That was the crucial value to which the figures obtained by expression (18) for all three analytical laws $P_N(u)$, $P_a(u)$, and $P_{a2}(u)$ were compared.

When this criterion is implemented, any deviation of the histogram p_i from theoretical function $P_T(u)$ will cause the X^2 estimation of inaccuracy to increase. This consists of systematic and random errors. The systematic error is a real divergence from the

prescribed data because of some factors not covered by the constructed model. The random error does not depend on what particular approximating function is used. This type of error is caused by a finite length of the data record and, according to the idea of goodness-of-fit testing, is expected to be less than χ_α^2. To verify this presumption the divergence (18) was estimated in such a way that a systematic error was absent. The X^2 function was calculated not between theoretical and experimental probability densities, as explained, but between two histograms for different data samples of the same strain signal used for the experimental curve in Fig. 8 (vertical gauge at the center of the plate under a sound pressure level of 154 dB). Because the result obtained, $X^2 = 29$, was not more than the tolerated value $\chi_{0.05}^2 = 32.7$, one can assume that, if it is exceeded during comparison of theoretical and experimental probability densities, the cause is a systematic error.

In this study, approximation is made in terms of distribution moments that precisely describe a probability density function only if their number approaches infinity. Thus, the systematic error cannot vanish entirely. For the normal law (3) based on variance σ^2 (the second moment M_2) only, the chi-square criterion (18) reaches a very high value, $X_N^2 = 780$, corresponding to the fundamental difference (see Fig. 8a) between the skewed experimental distribution (solid curve) and the symmetrical Gaussian probability density (dashed curve). Once the skewness value λ, related to the third moment M_3 by the first formula in Eq. (1), has been involved in the approximation process with assistance of the binormal law (13), the error of fitting decreased to $X_{a2}^2 = 259$ (solid and dashed curves came closer together in Fig. 8b than in Fig. 8a). Further improvement has been gained after implementation of the tetranormal law (9) provided additional simulation of kurtosis γ (the fourth moment M_4). The chi-square value obtained, $X_a^2 = 78$, appeared to be comparable to the aforementioned random error. It is natural that some systematic error still remains because the moments higher than fourth order have not been considered. This could be done if more than four sections were taken in the piecewise-Gaussian formula (8). However, in so doing the mathematical solution is inevitably complicated and, therefore, it was decided to stop at this stage with a supplementary reason that the experimental distribution and the theoretical data coincided satisfactorily (Fig. 8c).

The main advantage of the piecewise-Gaussian distributions lies in the fact that they are convenient for employment in subsequent analytical manipulations performed after processing experimental data. In many practical problems, one-dimensional probability densities are presented in the integrand as a cofactor to some function $F(u)$. For the normal law (3) with a zero mean value m, such integrals possess a form

$$I = \frac{1}{\sigma\sqrt{2\pi}} \int_{\tau_1}^{\tau_2} F(u) \exp\left(-\frac{u^2}{2\sigma^2}\right) \mathrm{d}u \tag{19}$$

When using piecewise-Gaussian probability densities (9), the integral spacing is broken into four sections, correspondingly,

$$I = \sum_{j=1}^{4} \int_{\psi_{j-1}}^{\psi_j} F(u) \frac{C}{\sigma\sqrt{2\pi}} \left\{ \exp\left[-\frac{(u-\sigma a_j)^2}{2\sigma^2 b_j}\right] + H_j \right\} \mathrm{d}u$$

with the following bounds: $\Psi_0 = \tau_1$, $\Psi_j = \sigma D_j$, $(j = 1, 2, 3)$, and $\Psi_4 = \tau_2$. Substituting the variables $w = (u - \sigma a_j)/\sqrt{b_j}$ with parameters a_j and b_j that depend on the section number j, we come to a relationship

$$I = \frac{C}{\sigma\sqrt{2\pi}} \sum_{j=1}^{4} \left\{ H_j \int_{\psi_{j-1}}^{\psi_j} F(u)\, \mathrm{d}u + \sqrt{b_j} \int_{\varphi_{j-1}^*}^{\varphi_j} \bar{F}(w) \exp\left(-\frac{w^2}{2\sigma^2}\right) \mathrm{d}w \right\} \tag{20}$$

where $\varphi_j = (\Psi_j - \sigma a_j)/\sqrt{b_j}$, $\varphi_j^* = (\Psi_j - \sigma a_{j+1})/\sqrt{b_{j+1}}$, and $\bar{F}(w) = F(\sqrt{b_j} w + \sigma a_j)$.

The expression (20) obtained has the same form of integrated functions as formula (19) for the Gaussian law. The only difference is that there are four integrals instead of one. Hence, it may be concluded that use of the developed piecewise-Gaussian distributions is reduced to repeated operations with exponential functions and, consequently, this does not cause basic difficulties compared with application of the normal law.

V. Peak Probability Distributions of Strain Response Processes

One of the most important problems in vibration analysis is fatigue life prediction. The time to failure of structural components under random loading depends on the peak probability density function of the dynamic response process. This function is usually described by the Rayleigh law

$$f(s) = (s/\sigma^2) \exp(-s^2/2\sigma^2) \tag{21}$$

assuming that the probability distribution of the response time history is close in form to the Gaussian law (3). The asymmetric abnormality of strain instantaneous-value probability distributions already discussed inevitably influences the peak probability density.

In the case when the dynamic response of a plate is dominated by one of its resonant modes, we can consider the strain response signal as a narrow-band stationary random process for which the number of zero crossings is approximately equal to the number of peak values. Under this condition the probability density of a peak of magnitude s can be expressed[15] as

$$f(s) = \frac{1}{R(0)} \left| \frac{\mathrm{d}R(s)}{\mathrm{d}s} \right| \tag{22}$$

in terms of the averaged number $R(s)$ of positive crossings of the level s by the strain response process $x(t)$. The function $R(s)$,

$$R(s) = \int_0^\infty v P_{x\dot{x}}(s, v)\, \mathrm{d}v \tag{23}$$

in turn depends on the two-dimensional joint probability density $P_{x\dot{x}}(u, v)$ of the strain process and its derivative $\dot{x}(t)$. Taking into consideration that, for a stationary random signal the processes $x(t)$ and $\dot{x}(t)$ are uncorrelated,[15] we assume, in addition, that $P_{x\dot{x}}(u, v)$ is equal to the product of the corresponding one-dimensional probability densities $P_x(u)$ and $P_{\dot{x}}(v)$. Because for the normal random process this is true, for non-Gaussian processes with reasonable distortions it can be taken as an approximate estimate. Then, the function $P_x(u)$ disappears from the integral in Eq. (23) and after substitution in Eq. (22) we have

$$f(s) = \frac{1}{P_x(0)} \left| \frac{\mathrm{d}P_x(u)}{\mathrm{d}u} \right|_{u=s} \tag{24}$$

where the peak probability density $f(s)$ of a strain process is defined by the distribution of instantaneous values $P_x(u)$ of its time history.

On approximating $P_x(u)$ by a piecewise-Gaussian distribution (9), the peak probability density becomes similarly constructed from shifted and scaled sections of a Rayleigh law distribution

$$f_a(s) = \begin{cases} \dfrac{|s-\sigma a_1|}{\sigma b_1 \{\exp[-a_k^2/(2b_k)] + H\}} \exp\left\{-\dfrac{(s-\sigma a_1)^2}{2\sigma^2 b_1}\right\} & \text{at} \quad s \le \sigma D_1 \\ \dfrac{|s-\sigma a_2|}{\sigma b_2 \{\exp[-a_k^2/(2b_k)] + H\}} \exp\left\{-\dfrac{(s-\sigma a_2)^2}{2\sigma^2 b_2}\right\} & \text{at} \quad \sigma D_1 < s \le \sigma D_2 \\ \dfrac{|s-\sigma a_3|}{\sigma b_3 \{\exp[-a_k^2/(2b_k)] + H\}} \exp\left\{-\dfrac{(s-\sigma a_3)^2}{2\sigma^2 b_3}\right\} & \text{at} \quad \sigma D_2 < s \le \sigma D_3 \\ \dfrac{|s-\sigma a_4|}{\sigma b_4 \{\exp[-a_k^2/(2b_k)] + H\}} \exp\left\{-\dfrac{(s-\sigma a_4)^2}{2\sigma^2 b_4}\right\} & \text{at} \quad s > \sigma D_3 \end{cases} \tag{25}$$

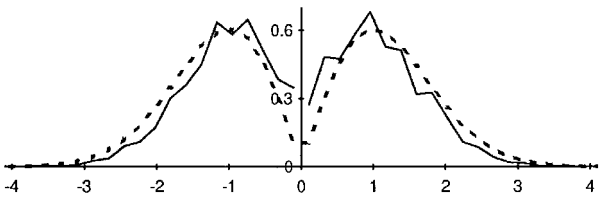

Fig. 9 Peak probability density function (——) of a strain signal with skewness $\lambda = 0.003$ and kurtosis $\gamma = 3.01$ (horizontal gauge near the plate clamp under 148-dB sound pressure level) compared to the Rayleigh law (– – –).

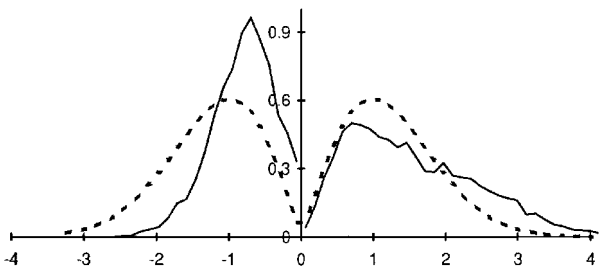

a) Experimental distribution (——) and the Rayleigh law (– – –)

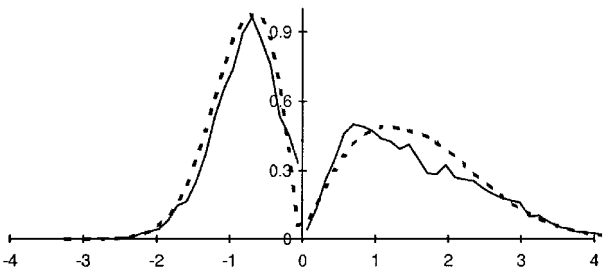

b) Experimental distribution (——) and piecewise-Rayleigh law (– – –)

Fig. 10 Peak probability density function of a strain signal with skewness $\lambda = 0.5$ and kurtosis $\gamma = 3.15$ (horizontal gauge at the center of the plate under 150-dB sound pressure level).

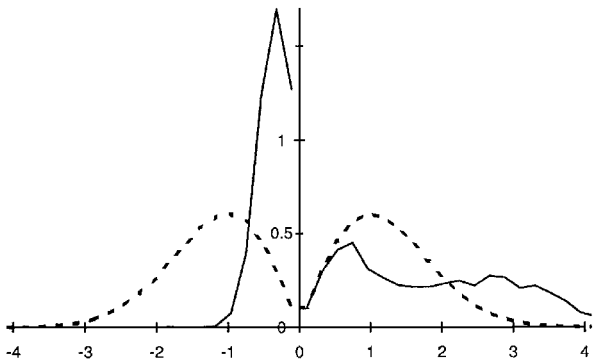

a) Experimental distribution (——) and the Rayleigh law (– – –)

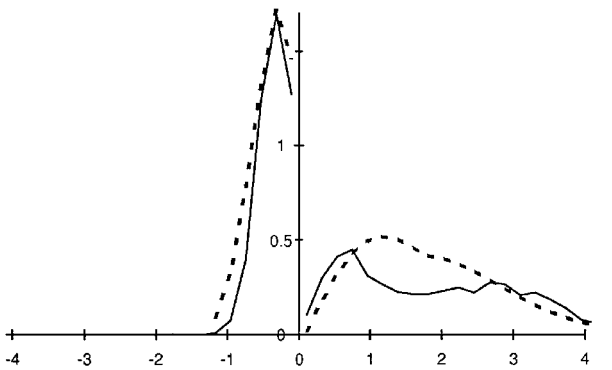

b) Experimental distribution (——) and piecewise-Rayleigh law (– – –)

Fig. 11 Peak probability density function of a strain signal with skewness $\lambda = 0.77$ and kurtosis $\gamma = 3.0$ (vertical gauge at the center of the plate under 156-dB sound pressure level).

where σ is the standard deviation of the strain process and $k = 2$ if the instantaneous-value distribution $P_x(u)$ has a negative skewness $\lambda < 0$ or $k = 3$ if $\lambda > 0$.

Because formula (25) has been derived on the basis of the simplified presentation of the joint probability density of a strain process $P_{x\dot{x}}(u, v) = P_x(u)P_{\dot{x}}(v)$, it is necessary to evaluate the accuracy of the solution obtained before using it in fatigue life prediction. For this purpose, extraction of maximum and minimum values has been performed from the strain time histories measured in the experiments that were described in Sec. II. Small cycles involving negative maxima and positive minima have been ignored in this process because they are not inherent in narrow-band random signals. The peak probability density functions were then calculated. They are presented in Figs. 9–11 by solid curves. Only the first, obtained for a low sound pressure level of 148 dB is close in form to the Rayleigh law (21) because the corresponding strain signal was a normal random process (see Fig. 3a).

The shapes of the other two peak distribution plots for 150 and 156 dB, similar to the instantaneous-value strain distributions discussed at the end of the second section, are the result of the one-sided, in-plane strain component. Because the in-plane strains are entirely positive, the total strain has more positive values than negative values. As a consequence, the maxima in the peak distribution are spread over a wider interval than the minima (see Fig. 6). However, the numbers of maxima and minima are the same. Hence, the shape of the minima probability distribution (solid curve for negative arguments in Figs. 10 and 11) is sharper than that of maxima (positive arguments).

Such behavior of peak probability density functions cannot be described by a symmetrical Rayleigh law (dashed curve in Figs. 10a and 11a) that corresponds to the usual Gaussian approximation (Fig. 8a) of the instantaneous-value probability density of strain processes. Formula (25) for the piecewise-Rayleigh distribution law permits better approximation of experimental peak probability densities. However, one should not ignore the influence that for a non-Gaussian strain process the joint probability density with its derivative is not strictly equal to the product of appropriate separate distributions as was assumed earlier. This difficulty has been overcome by the following two-stage calculation technique.

The first stage was approximation of the skewed instantaneous-value probability density of the measured strain record by the piecewise-Gaussian law (9). This procedure is based on strict mathematical tolls (see Sec. III) and gives satisfactory results (Fig. 8c). Distortions occur when the parameters α and β obtained are substituted into expression (25) for analytical peak probability density, which, because of the simplifying assumption made, appears to be different from the experimental peak distribution. However, at the second stage, a special iteration process was performed on the refinement of parameters α and β to fit the maxima of the analytical function (25) to the corresponding points of the experimental curve. As a result, satisfactory accuracy of the simulation of the peak distribution has been achieved (Figs. 10b and 11b).

Figure 10 displays the results of fitting a peak probability distribution (skewness value is 0.5) of the strain response signal from the horizontal gauge at the center of the plate under 150-dB excitation; the second example (Fig. 11) is for the vertical gauge under 156 dB producing a strain signal with higher skewness of 0.77. The final expression for the first piecewise-Rayleigh peak probability density (dashed curve in Fig. 10b) obtained after the two-stage approximation procedure is

$$f_a(s) =$$

$$\begin{cases} \dfrac{|s+0.62\sigma|}{0.42\sigma}\exp\left\{-\dfrac{(s+0.62\sigma)^2}{0.77\sigma^2}\right\} \\ \qquad\qquad \text{at} \quad s \le -1.24\sigma \\ \dfrac{|s+0.52\sigma|}{0.39\sigma}\exp\left\{-\dfrac{(s+0.52\sigma)^2}{0.71\sigma^2}\right\} \\ \qquad\qquad \text{at} \quad -1.24\sigma < s \le -0.52\sigma \\ \dfrac{|s+0.52\sigma|}{1.56\sigma}\exp\left\{-\dfrac{(s+0.52\sigma)^2}{2.87\sigma^2}\right\} \\ \qquad\qquad \text{at} \quad -0.52\sigma < s \le 0.92\sigma \\ \dfrac{|s+0.33\sigma|}{1.69\sigma}\exp\left\{-\dfrac{(s+0.33\sigma)^2}{3.1\sigma^2}\right\} \\ \qquad\qquad \text{at} \quad s > 0.92\sigma \end{cases}$$

Thus, the peak distribution model constructed has a form of four sections similar to the already considered instantaneous-value distribution (17). Therefore, it has the same advantage of convenience for use in subsequent analytical manipulations.

Conclusions

Experimental investigation was undertaken in a progressive wave tube of strain responses in carbon fiber-reinforced plates subjected to broadband random acoustic excitation typical of jet engine effluxes. Probability density functions of the dynamic processes studied appeared to be different from the generally used Gaussian law model for the instantaneous-value distribution and the Rayleigh law for the probability density of time history peaks. To describe these deviations of experimental data from the conventional theoretical models, the implications of using a piecewise approximation procedure have been examined, and an analytical solution on the basis of skewness and kurtosis distribution parameters has been obtained. The results are applicable for prediction of fatigue life of flight vehicle components. The approach to the problem appears to be promising because its application in practice does not cause basic difficulties as compared to the classical solutions using the Gaussian amplitude distribution and Rayleigh peak probability density.

Acknowledgments

The authors are very grateful to the Royal Society for support of their studies, particularly for the joint project grant provided for cooperation between scientists in the United Kingdom and the former Soviet Union. The results presented in the third section of the paper were obtained by the first author while sponsored by a Fellowship of the A. von Humboldt Foundation. The authors express their thanks to B. Benchekchou for help in running experiments.

References

[1]Mei, C., and Prasad, C. B., "Effects of Large Deflection and Transverse Shear on Response of Rectangular Symmetric Composite Laminates Subjected to Acoustic Loading," *Journal of Composite Materials*, Vol. 23, No. 6, 1989, pp. 606–639.

[2]Lowson, M. V., "Future Aerospace Use of Advanced Materials," *Proceedings of the Royal Aeronautical Society Conference on Aerospace Applications of Advanced Materials* (London), Royal Aeronautical Society, 1989, pp. 1.1–1.8.

[3]White, R. G., "Developments in the Acoustic Fatigue Design Process for Composite Aircraft Structures," *Composite Structures*, Vol. 16, No. 2, 1990, pp. 171–192.

[4]Mei, C., and Wentz, K. R., "Large Amplitude Random Response of Angle Ply Laminated Composite Plates," *AIAA Journal*, Vol. 20, No. 10, 1982, pp. 1450–1458.

[5]White, R. G., "A Comparison of Some Statistical Properties of the Responses of Aluminium Alloy and CFRP Plates to Acoustic Excitation," *Composites*, Vol. 9, No. 4, 1978, pp. 251–258.

[6]Wolfe, H. F., and White, R. G., "Experimental Studies of the Nonlinear Dynamic Behavior of Clamped-Clamped Aluminum and Carbon Fiber Reinforced Plastic Beams at Large Deflections," AIAA Paper 93-4336, Oct. 1993.

[7]Minguet, P., and Dugundji, J., "Experiments and Analysis for Composite Blades Under Large Deflections: Part 2 Dynamic Behavior," *AIAA Journal*, Vol. 28, No. 9, 1990, pp. 1580–1588.

[8]Kendall, M., and Stuart, A., "The Advanced Theory of Statistics," *Distribution Theory*, Vol. 1, Charles Griffin, London, 1963, Chap. 6.

[9]Crandall, S. H., "Non-Gaussian Closure Techniques for Stationary Random Vibration," *International Journal of Non-Linear Mechanics*, Vol. 20, No. 1, 1985, pp. 1–8.

[10]Steinwolf, A., "Approximation and Simulation of Probability Distributions with a Variable Kurtosis Value," *Computational Statistics and Data Analysis*, Vol. 21, No. 2, 1996, pp. 163–180.

[11]Steinwolf, A., "Analysis and Approximation of Probability Distribution of Vehicle Random Vibrations with Consideration of Kurtosis and Skewness Values," *Structural Dynamics: Recent Advances. Proceedings of 5th International Conference* (Southampton, England, UK), Inst. of Sound and Vibration Research, 1994, pp. 785–794.

[12]Richards, E. J., and Mead, D. J., *Noise and Acoustic Fatigue in Aeronautics*, Willey, London, 1968, p. 406.

[13]Steinwolf, A., *Analysis and Simulation of Non-Gaussian Random Vibrations*, Naukova Dumka, Kiev, 1993, Chap. 2 (in Russian).

[14]Bendat, J. S., and Piersol, A. G., *Random Data. Analysis and Measurement Procedures*, Wiley, New York, 1986, pp. 91–94.

[15]Lin, Y. K., *Probabilistic Theory of Structure Dynamics*, McGraw–Hill, New York, 1967, Chap. 9.

G. A. Kardomateas
Associate Editor